NANO LETTERS

Letter

pubs.acs.org/NanoLett

Electromagnetic Torque Tweezers: A Versatile Approach for Measurement of Single-Molecule Twist and Torque

Xander J. A. Janssen,† Jan Lipfert,† Tessa Jager, Renier Daudey, Jaap Beekman, and Nynke H. Dekker*

Department of Bionanoscience, Kavli Institute of Nanoscience, Delft University of Technology, Lorentzweg 1, 2628 CJ Delft, The Netherlands

Supporting Information

ABSTRACT: The well-established single-molecule force-spectroscopy techniques have recently been complemented by methods that can measure torque and twist directly, notably magnetic torque tweezers and the optical torque wrench. A limitation of the current torque measurement schemes is the intrinsic coupling between the force and torque degrees of freedom. Here we present electromagnetic torque tweezers (eMTT) that combine permanent and electromagnets to enable independent control of the force and torsional trap stiffness for sensitive measurements of single molecule torque and twist. Using the eMTT, we demonstrate sensitive torque measurements on tethered DNA molecules from simple tracking of the beads' (x,y)-position, obviating the need for any angular tracking algorithms or markers. Employing the eMTT for high-resolution torque measurements, we experimentally confirm the theoretically predicted torque overshoot at the DNA buckling transition in high salt conditions. We envision that the flexibility and control afforded by the eMTT will enable a range of new torque and twist measurement schemes from single-molecules to living cells.

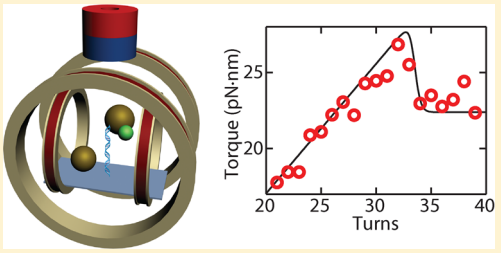

KEYWORDS: *Electromagnetic torque tweezers, torque spectroscopy, torsional stiffness, DNA supercoiling, DNA buckling*

Recently, the well-established single-molecule manipulation toolkit[1−3] has been complemented by methods that cannot only apply forces and measure extensions but also probe rotational motion and quantify torque. Single-molecule torque measurement schemes include magnetic torque tweezers (MTT)[4−7] that add that ability to directly measure torque to conventional magnetic tweezers and the optical torque wrench (OTW) that extends the capabilities of optical tweezers to the angular domain through polarization control and the use of birefringent particles.[8−13] Single-molecule torque and twist measurements have provided novel insights into the properties of twist storing polymers in particular of double-stranded DNA[5,8,14−16] and provide a sensitive probe of DNA processing by proteins,[5,17,18] as the double-helical nature of DNA intrinsically links processes such as DNA replication, transcription, and repair to build-up of torsional strain and the local accumulation of DNA supercoiling.

A drawback of currently available torque measurement schemes is the intrinsic coupling between the force and torque degrees of freedom: for example, current MTT instruments employ permanent magnets that control both the stretching force and the rotational trapping potential.[4,5] Similarly, varying the laser power in the OTW alters both the positional and rotational trap stiffness of the optical trap.[12] The torque tweezers scheme presented by Croquette and co-workers in principle decouples force and torque; however, it only achieves very low stretching forces.[6] Bryant and co-workers have developed a rotor bead assay that decouples force- and torque-generation by employing magnetic tweezers for the force application and a separate, nonmagnetic rotor bead for torque application and readout.[1,15,17,19,20] While achieving high torque and temporal resolution, the requirement for separate molecular attachment points for magnetic and rotor beads and the need for feedback control to achieve constant twist measurements[20] make this assay technically more challenging than traditional magnetic tweezers experiments.

To overcome these shortcomings, we introduce a novel MTT instrument, termed the electromagnetic torque tweezers (eMTT). The eMTT combine permanent and electromagnets to enable the application of a wide range of stretching forces (from <10 fN to tens of pN), while independently controlling the torsional trap stiffness of the instrument (from zero up to several pN·μm/rad). Independent control of force and torsional trap stiffness is desirable for several reasons. First, for torque measurements it is advantageous to match the torsional trap stiffness of the instrument to the characteristic torques of the molecule or molecular complex under study. If the trap is too soft, it becomes difficult to apply sufficient torque to fully probe the response of the system. If, on the other hand, the trap is too stiff, the restoring torques exerted by the macromolecule lead to only very small displacements from the equilibrium position of the rotational trap, which precludes accurate torque measurements.[5,7] Second, being able to rapidly change trap stiffness affords experimental flexibility, for

Received: April 8, 2012
Revised: May 23, 2012

   dx.doi.org/10.1021/nl301330h | *Nano Lett.* XXXX, XXX, XXX−XXX

example, to alternate between rapid changes of molecular twist (using a high trap stiffness) and sensitive torque measurements (using a lower trap stiffness). Third, recent theoretical work suggests that, at least in principle, the torque measured in single-molecule experiments can depend on the torsional trap stiffness of the measurement apparatus.[21]

In this Letter, we show how the eMTT afford independent control of force and torsional trap stiffness and present torque measurements on DNA molecules tethered between superparamagnetic beads and a flow cell surface at different trap stiffness. In particular, we demonstrate sensitive torque measurements on DNA from simple readout of the beads' (x,y)-positions without the need for a specialized angular tracking protocol. Finally, we employ the high-resolution torque measurement capabilities of the eMTT to experimentally confirm the theoretically predicted[14,21,22] torque overshoot at the DNA buckling transition.

At the center of the eMTT are superparamagnetic beads connected to a flow cell surface by double-stranded DNA tethers (Figure 1a,b), similar to standard MT instruments.[23,24] A vertically oriented cylindrical magnet mounted above the flow cell exerts a magnetic field that is symmetric about the z-axis and provides a strong field gradient in the z-direction. The field gradient of this permanent magnet gives rise to an upward force on the magnetic beads and thus exerts a stretching force on the DNA tethers,[7,25,26] which can be controlled by adjusting the height of the magnet above the flow cell with a vertical linear stage. With the magnetic field aligned vertically, the preferred magnetization axis of the bead m_0 aligns vertically as well and the rotation of the bead around the tether is not constrained by the magnet (Figure 1c). In this geometry, termed freely orbiting magnetic tweezers (FOMT),[26] the thermal motion of the bead's center traces out a circular annulus in (x,y) as a consequence of the free rotation about the tether point (Figure 1c, right panel). The radius of the circular annulus R_{circle} depends on the attachment point of the DNA tether on the bead and lies between zero (for attachment at the south pole) and $\sim R_{bead}$ (for attachment at the equator).[26] The (x,y)-position of the bead on the circular annulus can be converted to radial and angular coordinates (R,θ), which effectively allows us to follow bead rotation from simple tracking of the (x,y)-positions (Supporting Information and Figure 1c). Alternatively, the bead's rotation can be tracked using an explicit angular tracking protocol based on attaching small fiducial marker beads to the larger magnetic bead and following their rotation[5,27] (see below). The upward stretching force on the tether can be calibrated from the width of the radial fluctuations $\langle \delta R^2 \rangle$ by adapting the approach used in conventional magnetic tweezers[23,26,28]

$$F = \frac{k_B T L}{\langle \delta R^2 \rangle} \quad (1)$$

where k_B is Boltzmann's constant, T is the absolute temperature, and L is the length of the tether. The stretching forces determined from eq 1 are in good agreement with values calculated from first principles by computing the magnetic field and taking into account the bead's magnetization[25,26] (Supporting Information and Supporting Information Figures S1−3).

The flow cell is at the center of two pairs of magnetic coils (Figure 1a,b) that are arranged approximately in Helmholtz geometry, i.e. with the distance between the coils equal to their radius. By running a current through the coils, we can apply homogeneous fields in the (x,y)-plane (Supporting Information and Supporting Information Figure S4). Applying a magnetic field $B_{Helmholtz}$ in the (x,y)-plane breaks the symmetry of the vertical field of the permament magnet $B_{permanent}$ and tilts the resulting field B_{sum} away from the z-axis (Figure 1d, left panel). This tilted field constrains the free rotation of the bead around the tether axis and leads to an effective torsional clamp in the direction of the applied field, constraining the thermal fluctuations of the bead to a segment of the circular annulus (Figure 1d, right panel). The trap stiffness of the rotational trap k_θ exerted by the Helmholtz field can be calibrated from the width of the thermal fluctuations $\langle \delta\theta^2 \rangle$

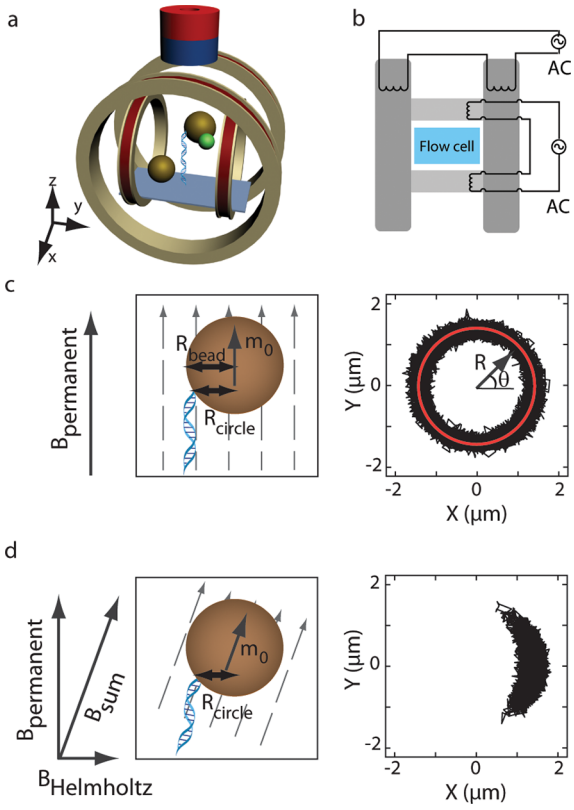

Figure 1. Experimental design and the orientation of DNA-tethered beads in the eMTT. (a) Schematic representation of a superparamagnetic bead tethered to a flow cell surface by a DNA molecule. A fixed reference bead is used to correct for drift. A cylindrically shaped permanent magnet positioned over the bead applies a vertically oriented force while leaving the bead rotationally unconstrained about the z-axis, i.e., the tether axis. The flow cell and permanent magnet are placed within four coils that apply homogeneous in-plane fields. (b) Schematic of the four coils (gray) surrounding the flow cell, together with their electrical connections. (c) A magnetic bead with a preferred magnetization axis m_0 is tethered to a DNA at a point between its south pole and the equator. The magnetic moment aligns with the local field direction of the permanent magnet ($B_{permanent}$). As this field is cylindrically symmetric, changes in the twist of the DNA tether that result from thermal fluctuations cause the bead to rotate about its tether point. As a consequence, the center of the bead traces out a circular annulus. Fitting a circle (red line) to the (x,y)-positions, one can perform a coordinate transformation of the measured positions from (x,y) to (R,θ). (d) Applying a horizontally oriented Helmholtz field ($B_{Helmholtz}$) results in a tilted magnetic field (B_{sum}) that effectively clamps the bead in the direction of the Helmholtz field, causing the bead's center to trace out only a segment of the circular annulus.

dx.doi.org/10.1021/nl301330h | Nano Lett. XXXX, XXX, XXX−XXX

$$k_\theta = \frac{k_B T}{\langle \delta\theta^2 \rangle} \quad (2)$$

The Helmholtz coils enable precise control over the bead's rotation about the tether axis. Applying a rotating field with the Helmholtz coils, the bead faithfully follows the rotation (Figure 2a). Clamping the field in fixed directions, the mean position of the bead is precisely constrained to the direction of the field (Figure 2b,c). We find the angular trap stiffness computed from the width of the angular fluctuations (eq 2) to be independent of the angular direction of the trap (Figure 1d and Supporting Information Figure S5), indicating that the two pairs of Helmholtz coils are well balanced, that is, that changing the field orientation does not change the field strength. In addition, we find the stretching force determined from the radial fluctuations (eq 1; Figure 1d and Supporting Information Figure S5) to be independent of field orientation. Using the Helmholtz coils to systematically rotate the bead around the tether axis, we reproduce the well-known rotation-extension response[23,29] of torsionally constrained double-stranded DNA tethers (Supporting Information Figure S6).

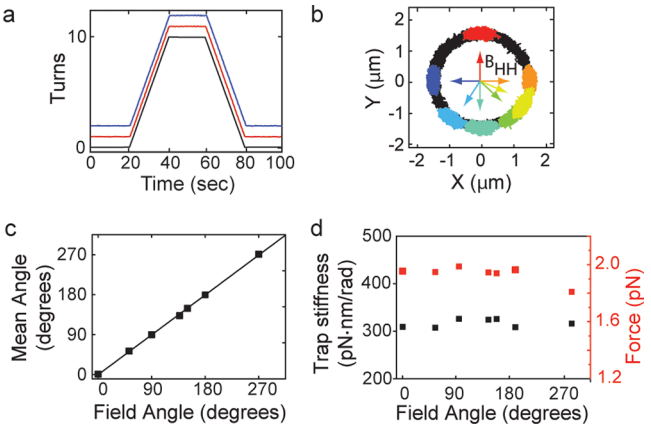

Figure 2. Controlling DNA-tethered bead rotation by rotating the Helmholtz field. (a) The Helmholtz field direction (black line) was rotated by 10 turns, held stationary, and rotated by −10 turns. During the stationary phase, the field was maintained at constant magnitude and direction. The bead's angular orientation (red and blue lines, offset by +1 and +2 turns for clarity) faithfully follows the direction of the applied field. Bead angles determined via (x,y) to (R,θ) coordinate transformation (red) are in excellent agreement with those determined via fiducial marker bead tracking (blue). (b) In absence of the Helmholtz field, the bead's center traces out a full circle (black points). The application of a Helmholtz field in a particular direction (colored arrows) traps the bead in the direction of this field (colored data sets). (c) The mean angular orientation of the bead (black squares) shows a 1:1 correspondence with the angular orientation of the applied field. The solid line is a linear fit through zero with a slope of 1.00 ± 0.01. (d) The in-plane applied torsional trap stiffness (black squares) and the vertically applied force (red squares) are independent of Helmholtz field orientation.

A key advantage of the eMTT over conventional MT instruments is that the torsional trap stiffness can be dialed in by changing the Helmholtz field at any given stretching force set by the position of the permanent magnet. For a given position of the permanent magnet and direction of the Helmholtz field, the width of the angular fluctuations decreases upon increasing the magnitude of the Helmholtz field (Figure 3a,b), while the width of the radial fluctuations and thus the stretching force remains constant (Supporting Information Figure S7). At a given stretching force, the torsional trap stiffness computed from the width of the angular fluctuations (eq 2) increases linearly with applied Helmholtz field, from effectively zero at zero field (corresponding to the FOMT geometry) to values in the range of ∼1000 pN·nm/rad at the highest fields achievable in our instrument (Figure 3d). Analyzing the Brownian motion of the bead in the angular trap exerted by the Helmholtz coils, we find that the temporal autocorrelations show an exponential decay with a characteristic time τ_C that is inversely proportional to the trap stiffness $\tau_C = \gamma/k_\theta$, where γ is the rotational friction coefficient[26] (Figure 3c, and below). We note that the angular traces in Figure 3 were obtained by using an explicit angular tracking protocol based on attaching a small fiducial marker bead to the larger magnetic bead[5,27] (Supporting Information). We find close agreement between the direct angle tracking protocol and the angular traces determined by converting the (x,y) position to (R,θ) at low and intermediate trap stiffness. At high trap stiffness, $k_\theta >$ 300 pN·nm/rad, the angle traces obtained from the coordinate transformation systematically overestimate the width of the angular fluctuations due to cross talk between (x,y) and angle fluctuations (Supporting Information and Supporting Information Figure S8). The ability to accurately track angle by simply tracking (x,y)-position at low and intermediate trap stiffness presents a experimental simplification compared to the explicit angle tracking protocol, since it avoids the need to add fiducial marker beads and to employ specialized tracking software.

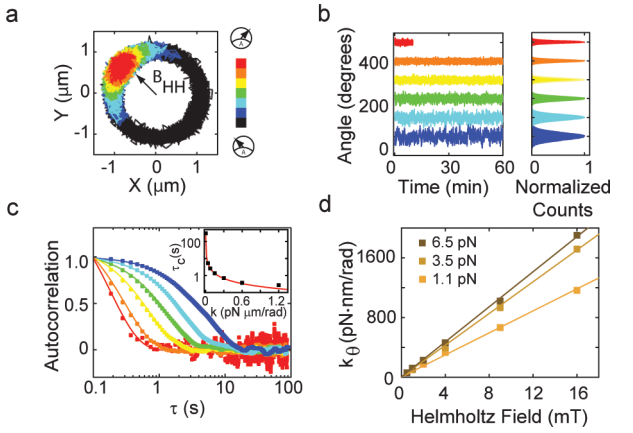

Figure 3. Tunability of torsional trap stiffness by varying the Helmholtz field amplitude. (a) The circular annulus traced out by the bead's center at zero transverse applied field, is compressed into increasingly smaller arcs with increasing Helmholtz field. From black to red, the magnitude of the applied Helmholtz field is 0, 0.5 1, 2, 4, 8, and 16 mT. (b) Time traces and corresponding histograms of the bead's angular orientation (measured with a fiducial marker) for Helmholtz fields of increasing amplitudes (color coding as in panel a). Successive data sets are vertically offset by +100 degrees for clarity. The measurement at 16 mT field was switched off after 8 min to prevent overheating of the Helmholtz coils. (c) The temporal autocorrelations of the measured time traces (panel b) show an exponential decay with a characteristic time τ_C that is inversely proportional (inset) to the trap stiffness $\tau_C = \gamma/k_\theta$, where γ is the rotational friction coefficient. (d) At a given stretching force, the torsional trap stiffness increases linearly with the applied Helmholtz field, from effectively zero at zero field to values in the range of ∼1000 pN·nm/rad at the highest fields achievable in our instrument.

We demonstrate the potential of our eMTT by performing systematic torque measurements on a 7.9 kbp DNA construct

dx.doi.org/10.1021/nl301330h | Nano Lett. XXXX, XXX, XXX−XXX

(Supporting Information). The torque measurement is based on stepwise over- and underwinding the DNA tether while precisely measuring the bead's angular orientation.[4,5] Starting with a torsionally relaxed tether, we measure the equilibrium position of the torque trap θ_0 (Figure 4a,b). After over- or underwinding the tether by an integral number of turns N, the DNA exerts a restoring torque on the bead, which causes the mean angular orientation to shift to a new position θ_N (Figure 4a,b). Having calibrated the torsional trap stiffness k_θ from eq 2, the torque exerted by the molecule can be directly determined as

$$\tau_{DNA} = -k_\theta \langle \theta_N - \theta_0 \rangle \quad (3)$$

Using this approach, we performed two torque measurements on the same 7.9 kb DNA tether at a stretching force of F = 3.5 pN using 2.8 μm diameter M270 beads in PBS+ buffer (Supporting Information) at two different magnitudes of the Helmholtz field (0.8 and 1.9 mT), corresponding to different values of the torsional trap stiffness. In both measurements the torsionally relaxed tether at 0 turns was first overwound by 75 turns in steps of 5 turns, then underwound by −40 turns, and finally rotated back to equilibrium, that is, 0 turns. Every 5 turns, the rotating field was maintained stationary and the angular fluctuations where measured for 400 s to determine mean angular orientation of the bead and the standard deviation of the angular distribution. Over the course of a torque measurement, the trap stiffness is found to be constant, that is, independent of the number of turns (Figure 4b). The constant trap stiffness allows changes in angular orientation (Figure 4c) to be converted directly to torque using eq 3 (Figure 4d). In both the high (Figure 4c, red data) and low (Figure 4c, blue data) torsional trap stiffness measurements, we consistently observe DNA denaturation, corresponding to the torque plateau at negative turns, at ∼−10.5 pN·nm, and DNA buckling, corresponding to the torque plateau at positive turns, at ∼30 pN·nm, which is in excellent agreement with previous measurements.[5] The buckling transition and subsequent formation of plectonemes is also visible as a decrease in the measured extension of the molecule (Figure 4e). Fitting the linear part of the torque vs turns curve (Figure 4d), we obtained a torsional stiffness of 95 ± 10 pN·nm at 0.8 mT and 97 ± 6 pN·nm at 1.9 mT, again in close agreement to previous measurements.[5] At the typical trap stiffnesses used for torque measurements both direct angle tracking and angle tracking from the (x,y) position give similar results (Supporting Information Figure S9).

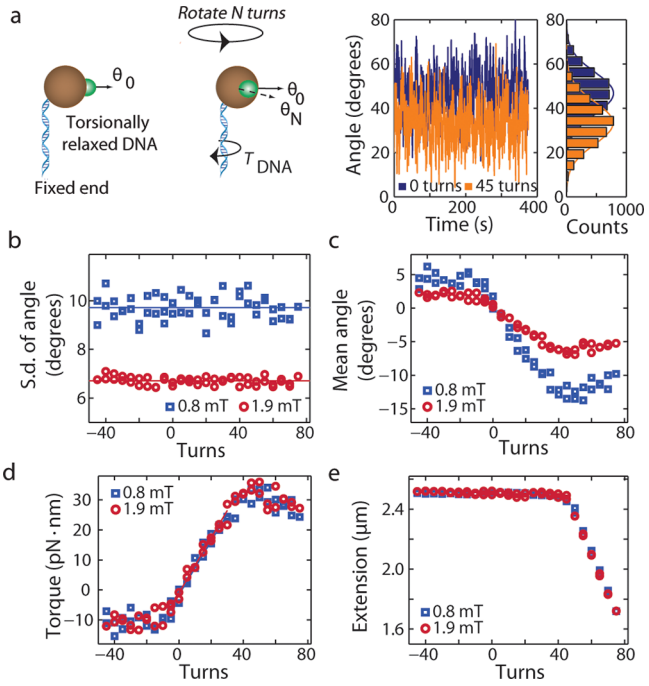

Figure 4. Flexibility in torque measurement strategies in the eMTT. (a) Left: Schematic representation of the principle of torque measurement, here shown using a marker bead (green) to report on the bead's angular position. Right: Time traces and corresponding histograms of the bead's angular orientation for a DNA molecule at N = 0 (torsionally relaxed, blue data) and at N = 45 (orange data). The angular shift of the histogram can be readily observed. (b−e) Measurement series of the torque stored in a 7.9 kbp DNA molecule versus the applied number of turns N, conducted at two values of the Helmholtz field, and hence at different torsional trap stiffnesses (all blue data measured at 0.8 mT; all red data measured at 1.9 mT). (b) The standard deviation of the bead's angular orientation is independent of the number of applied turns both at low (blue squares) and high (red circles) trap stiffness. (c) The measured mean angle θ_N (relative to θ_0) versus the number of applied turns. The magnitude of the angular shift decreases with increasing trap stiffness. (d) The torque stored in the DNA molecule versus the number of applied turns. (e) The extension of the DNA molecule versus the number of applied turns.

Simple theories of the buckling transition and plectoneme formation in DNA predict a linear increase in torque with increasing twist up to the buckling point and constant torque after the buckling point in the plectonemic region.[3,29−31] At least qualitatively, previous torque measurements have been consistent with a linear increase in torque with increasing number of turns up to the buckling transition and a constant torque plateau postbuckling[4,5,8] (Figure 4). Recently, however, more refined theories of the buckling transition have predicted a "torque overshoot", that is, with increasing number of turns, the torque is predicted to first increase linearly, then decrease sharply at the buckling transition and finally assume a postbuckling plateau value.[14,21,22] This torque overshoot is associated with a sharp decrease in the DNA extension at the buckling transition. Fundamentally, both the sharp decrease in DNA extension and the overhoot of the torque are due to the fact that the first loop in the plectoneme has a different geometry and higher energy cost than the subsequent plectonemic loops.[14,21,22] Even though the current models differ in the details of their predictions about the sudden change in extension and torque, both effects are generally predicted to depend on stretching force and in particular ionic strength of the buffer. While the rapid change in extension at the buckling point has been experimentally studied in detail,[8,22] there has only been one very recent experimental observation of the theoretically predicted torque overshoot.[20]

To investigate the changes in torque at the DNA buckling transition, we increased the resolution of our torque measurements by employing smaller beads together with the (x,y)-tracking based angle measurements that allow measurements without fiducial marker beads. We note that decreasing the rotational friction coefficient γ by decreasing the bead radius or measuring with a higher trap stiffness both decrease the characteristic time $\tau_c = \gamma/k_\theta$ of angular fluctuations (Figures 3c and 5a) and, therefore, decrease the time resolution to detect changes in angle. However, increasing the trap stiffness does not increase the torque resolution per measurement time.[5] In

dx.doi.org/10.1021/nl301330h | Nano Lett. XXXX, XXX, XXX−XXX

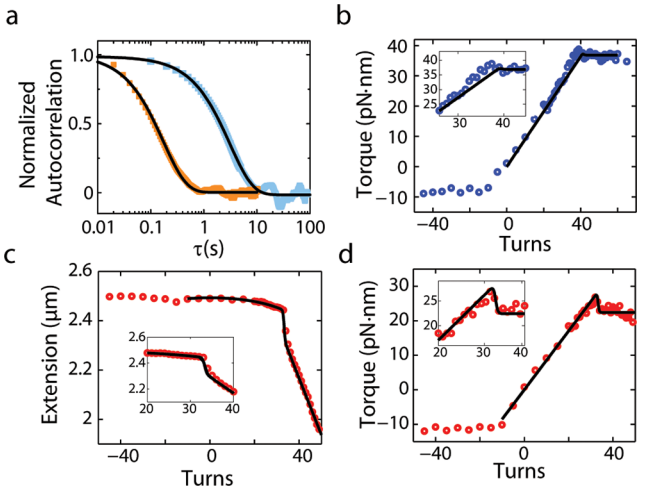

Figure 5. Demonstration of an overshoot in the DNA torque at the buckling transition. (a) The autocorrelation of the measured angular orientation in time for a 2.8 μm M270 bead measured at a trap stiffness of 66 pN·nm/rad (blue squares) shows an exponential decay with a characteristic time of 3.1 s (fit to a single exponential, black line). The autocorrelation of the measured angular orientation in time for a 1 μm MyOne bead measured at a trap stiffness of 52 pN·nm/rad (orange squares) shows a similar decay with a characteristic time of 0.17 s (fit to single exponential decay, black line). The corresponding rotational friction coefficients are 202 pN·nm·s (2.8 μm bead) and 9 pN·nm·s (1 μm bead); their ratio is in good agreement with the cubed ratio of the bead radii. (b–d) Torque and extension measurements as a function of applied turns on a 7.9 kbp DNA using 1.0 μm beads. (b) At a low salt condition (20 mM monovalent), no significant torque overshoot is observed at the buckling transition, which is in agreement with a model of DNA buckling (solid black line and Supporting Information). (c) The measured extension versus number of turns at high salt (550 mM monovalent) shows a sharp decrease at the buckling transition, which is in good agreement with a model of DNA extension (solid black line and Supporting Information). (d) At a high salt condition (550 mM monovalent), a torque overshoot is readily discernible at the buckling transition, which is in good agreement with the overshoot predicted by the model (black line and Supporting Information).

the limit that the measurement is not limited by tracking errors or instrument drift, the torque resolution (σ_τ) is given by $\sigma_\tau = (k_B T\, \gamma/t_{meas})^{1/2}$, where t_{meas} is the measurement time.[5] As the rotational friction coefficient γ increases with the third power of the bead radius,[26] using 1.0 μm beads (Figure 5a, orange data) instead of 2.8 μm beads (Figure 5a, blue data) decreases γ and thus τ_c approximately $(2.8/1)^3 \sim$ 22-fold. Consequently, this reduction in bead size increases the torque resolution for a given measurement time by approximately $(2.8/1)^{3/2} \sim$ 5-fold. A drawback of using smaller beads is the reduction in stretching force that can be applied, as the force scales with the bead volume. To (partially) compensate the reduction in bead volume, we used a stack of three magnets of which the bottom one is stacked with opposite magnetization direction giving rise to higher gradient forces than the standard cylindrical magnet.[7]

Using 1.0 μm diameter beads held in the eMTT at a relatively low trap stiffness of ~50 pN·nm/rad, we performed systematic torque measurements on our 7.9 kbp DNA constructs at low (20 mM monovalent salt) and high salt concentration (550 mM monovalent) at a stretching force of F = 3.5 pN. At the low salt concentration, we observe no or only a small torque overshoot (<2 pN·nm), which is in agreement with a semiquantitative model of the DNA buckling transition (Figure 5b; for details of the model, see Supporting Information). In contrast, at the high salt condition the model predicts a torque overshoot of ~5 pN·nm and the effect is readily discernible in the experimental data (Figure 5c,d and Supporting Information Figure S10), where we observe a torque overshoot of 4 ± 1 pN·nm (mean and SD of five biological repeats).

In summary, we have demonstrated that eMTT enable independent control of the stretching force and torsional trap stiffness in single-molecule measurements of torque and twist. This flexibility is achieved by combining a cylindrical permanent magnet with two pairs of Helmholtz coils. Using the eMTT, we have performed high-resolution torque measurements on double-stranded DNA that confirm the theoretically predicted torque overshoot at the buckling transition at high salt concentration. We envision that the eMTT will provide a flexible platform for single-molecule measurements, whereby the ability to accurately and rapidly control the in-plane field with the Helmholtz coils makes it possible to sensitively bias the rotational energy landscape experienced by the magnetic beads (Supporting Information Figure S11) and will open up new types of feedback on torque measurements. Alternatively, the eMTT have the potential to be used to characterize the viscous and elastic properties of soft matter such as polymer gels or living cells,[32,33] relying on the readout of a particle's thermal fluctuations[34,35] or on controlled motion[13,32,33,36] to report on, for example, loss processes, viscosity, and shear moduli. Whereas currently available techniques employing optical tweezers[13,36] have only limited ability to control multiple particles, magnetic tweezers techniques are perfectly suited for parallelization.[37−39] Controlled manipulation of large ensembles of magnetic particles using homogeneous magnetic fields as in the eMTT facilitates their use as colloidal modal systems[40] and applicability in magnetic biosensor applications[41] or targeted drug delivery.[42]

■ ASSOCIATED CONTENT

Supporting Information

Additional figures and information. This material is available free of charge via the Internet at http://pubs.acs.org.

■ AUTHOR INFORMATION

Corresponding Author

*E-mail: N.H.Dekker@tudelft.nl.

Author Contributions

†Equal contribution.

Notes

The authors declare no competing financial interest.

■ ACKNOWLEDGMENTS

We thank the members of our laboratory for stimulating discussions, Hugh van der Kolff and Rafael Doelwijt for help with initial measurements, Jelle van der Does and Dimitri de Roos for help with instrumentation, Jacob Kerssemakers for help with tracking, Susanne Hage and Serge Donkers for providing the DNA constructs, and An Prenen for help in drawing Figure 1a. This work was supported by the Netherlands Organization for Scientific Research (NWO), the European Science Foundation, the Foundation for Fundamental Research on Matter (FOM) and by Delft University of Technology.

REFERENCES

(1) Bustamante, C.; Bryant, Z.; Smith, S. B. *Nature* **2003**, *421* (6921), 423−427.
(2) Neuman, K. C.; Nagy, A. *Nat Methods* **2008**, *5* (6), 491−505.
(3) Strick, T.; Allemand, J.; Croquette, V.; Bensimon, D. *Prog. Biophys. Mol. Biol.* **2000**, *74* (1−2), 115−40.
(4) Celedon, A.; Nodelman, I. M.; Wildt, B.; Dewan, R.; Searson, P.; Wirtz, D.; Bowman, G. D.; Sun, S. X. *Nano Lett.* **2009**, *9* (4), 1720−5.
(5) Lipfert, J.; Kerssemakers, J. W.; Jager, T.; Dekker, N. H. *Nat. Methods* **2010**, *7* (12), 977−80.
(6) Mosconi, F.; Allemand, J. F.; Croquette, V. *Rev. Sci. Instrum.* **2011**, *82* (3), 12.
(7) Kauert, D. J.; Kurth, T.; Liedl, T.; Seidel, R. *Nano Lett.* **2011**, *11* (12), 5558−63.
(8) Forth, S.; Deufel, C.; Sheinin, M. Y.; Daniels, B.; Sethna, J. P.; Wang, M. D. *Phys. Rev. Lett.* **2008**, *100* (14), 148301.
(9) Gutierrez-Medina, B.; Andreasson, J. O.; Greenleaf, W. J.; Laporta, A.; Block, S. M. *Methods Enzymol.* **2010**, *475*, 377−404.
(10) Huang, Z.; Pedaci, F.; van Oene, M.; Wiggin, M. J.; Dekker, N. H. *ACS Nano* **2011**, *5* (2), 1418−27.
(11) Inman, J.; Forth, S.; Wang, M. D. *Opt. Lett.* **2010**, *35* (17), 2949−51.
(12) La Porta, A.; Wang, M. D. *Phys. Rev. Lett.* **2004**, *92* (19), 190801.
(13) Pedaci, F.; Huang, Z. X.; van Oene, M.; Barland, S.; Dekker, N. H. *Nat. Phys.* **2011**, *7* (3), 259−264.
(14) Daniels, B. C.; Forth, S.; Sheinin, M. Y.; Wang, M. D.; Sethna, J. P. *Phys. Rev. E Stat., Nonlinear Soft Matter Phys.* **2009**, *80* (4 Pt 1), 040901.
(15) Gore, J.; Bryant, Z.; Nollmann, M.; Le, M. U.; Cozzarelli, N. R.; Bustamante, C. *Nature* **2006**, *442* (7104), 836−9.
(16) Sheinin, M. Y.; Forth, S.; Marko, J. F.; Wang, M. D. *Phys. Rev. Lett.* **2011**, *107* (10), 108102.
(17) Gore, J.; Bryant, Z.; Stone, M. D.; Nollmann, M. N.; Cozzarelli, N. R.; Bustamante, C. *Nature* **2006**, *439* (7072), 100−104.
(18) Harada, Y.; Ohara, O.; Takatsuki, A.; Itoh, H.; Shimamoto, N.; Kinosita, K., Jr. *Nature* **2001**, *409* (6816), 113−5.
(19) Basu, A.; Schoeffler, A. J.; Berger, J. M.; Bryant, Z. *Nat. Struct. Mol. Biol.* **2012**, *19* (5), 538−46.
(20) Oberstrass, F. C.; Fernandes, L. E.; Bryant, Z. *Proc. Natl. Acad. Sci. U.S.A.* **2012**, *109* (16), 6106−6111.
(21) Marko, J. F.; Neukirch, S. *Phys Rev E Stat Nonlin Soft Matter Phys* **2012**, *85* (1−1), 011908.
(22) Brutzer, H.; Luzzietti, N.; Klaue, D.; Seidel, R. *Biophys. J.* **2010**, *98* (7), 1267−76.
(23) Strick, T. R.; Allemand, J. F.; Bensimon, D.; Bensimon, A.; Croquette, V. *Science* **1996**, *271* (5257), 1835−1837.
(24) Vilfan, I. D.; Lipfert, J.; Koster, D. A.; Lemay, S. G.; Dekker, N. H. Magnetic Tweezers for Single-Molecule Experiments. In *Handbook of Single-Molecule Biophysics*; Hinterdorfer, P., van Oijen, A., Eds.; Springer: New York, 2009.
(25) Lipfert, J.; Hao, X.; Dekker, N. H. *Biophys. J.* **2009**, *96* (12), 5040−9.
(26) Lipfert, J.; Wiggin, M.; Kerssemakers, J. W.; Pedaci, F.; Dekker, N. H. *Nat. Commun.* **2011**, *2*, 439.
(27) Lipfert, J.; Kerssemakers, J. J.; Rojer, M.; Dekker, N. H. *Rev. Sci. Instrum.* **2011**, *82* (10), 103707.
(28) te Velthuis, A.; Kerssemakers, J. W. J.; Lipfert, J.; Dekker, N. H. *Biophys. J.* **2010**, *99* (4), 1292−1302.
(29) Strick, T. R.; Dessinges, M. N.; Charvin, G.; Dekker, N. H.; Allemand, J. F.; Bensimon, D.; Croquette, V. *Rep. Prog. Phys.* **2003**, *66* (1), 1−45.
(30) Marko, J. F. *Phys. Rev. E* **2007**, *76* (2 Pt 1), 021926.
(31) Mosconi, F.; Allemand, J. F.; Bensimon, D.; Croquette, V. *Phys. Rev. Lett.* **2009**, *102* (7), 078301.
(32) de Vries, A. H. B.; Krenn, B. E.; van Driel, R.; Kanger, J. S. *Biophys. J.* **2005**, *88* (3), 2137−2144.
(33) de Vries, A. H. B.; Krenn, B. E.; van Driel, R.; Subramaniam, V.; Kanger, J. S. *Nano Lett.* **2007**, *7* (5), 1424−1427.
(34) Gittes, F.; Schnurr, B.; Olmsted, P. D.; MacKintosh, F. C.; Schmidt, C. F. *Phys. Rev. Lett.* **1997**, *79* (17), 3286−3289.
(35) Schnurr, B.; Gittes, F.; MacKintosh, F. C.; Schmidt, C. F. *Macromolecules* **1997**, *30* (25), 7781−7792.
(36) Liu, Q.; Asavei, T.; Lee, T.; Rubinsztein-Dunlop, H.; He, S.; Smalyukh, I. I. *Opt. Express* **2011**, *19* (25), 25134−U1043.
(37) Ribeck, N.; Saleh, O. A. *Rev. Sci. Instrum.* **2008**, *79*, 094301.
(38) De Vlaminck, I.; Henighan, T.; van Loenhout, M. T. J.; Pfeiffer, I.; Huijts, J.; Kerssemakers, J. W. J.; Katan, A. J.; van Langen-Suurling, A.; van der Drift, E.; Wyman, C.; Dekker, C. *Nano Lett.* **2011**, *11* (12), 5489−5493.
(39) Plénat, T.; Tardin, C.; Rousseau, P.; Salomé, L. *Nucleic Acids Res.* **2012**.
(40) Ebert, F.; Dillmann, P.; Maret, G.; Keim, P. *Rev. Sci. Instrum.* **2009**, *80* (8), 083902.
(41) Ranzoni, A.; Schleipen, J.; van Ijzendoorn, L. J.; Prins, M. W. J. *Nano Lett.* **2011**, *11* (5), 2017−2022.
(42) Ghosh, A.; Fischer, P. *Nano Lett.* **2009**, *9* (6), 2243−2245.